Anharmonic Eigenvectors and Acoustic Phonon Disappearance in Quantum Paraelectric $SrTiO_3$

Xing He,[1] Dipanshu Bansal,[2] Barry Winn,[3] Songxue Chi,[3] Lynn Boatner,[4] and Olivier Delaire[1,5,6,*]
[1]Mechanical Engineering and Materials Science, Duke University, Durham, North Carolina 27708, USA
[2]Department of Mechanical Engineering, Indian Institute of Technology Bombay, Mumbai, Maharashtra 400076, India
[3]Neutron Scattering Directorate, Oak Ridge National Laboratory, Oak Ridge, Tennessee 37831, USA
[4]Materials Science and Technology Division, Oak Ridge National Laboratory, Oak Ridge, Tennessee 37831, USA
[5]Department of Physics, Duke University, Durham, North Carolina 27708, USA
[6]Department of Chemistry, Duke University, Durham, North Carolina 27708, USA

(Received 10 September 2019; revised manuscript received 19 January 2020; accepted 16 March 2020; published 9 April 2020)

Pronounced anomalies in the $SrTiO_3$ dynamical structure factor, $S(\mathbf{Q}, E)$, including the disappearance of acoustic phonon branches at low temperatures, were uncovered with inelastic neutron scattering (INS) and simulations. The striking effect reflects anharmonic couplings between acoustic and optic phonons and the incipient ferroelectric instability near the quantum critical point. It is rationalized using a first-principles renormalized anharmonic phonon approach, pointing to nonlinear Ti-O hybridization causing unusual changes in real-space phonon eigenvectors, frequencies, group velocities, and scattering phase space. Our method is general and establishes how T dependences beyond the harmonic regime, assessed by INS mapping of large reciprocal-space volumes, provide real-space insights into anharmonic atomic dynamics near phase transitions.

DOI: 10.1103/PhysRevLett.124.145901

An archetypical perovskite, $SrTiO_3$ (STO) has attracted interest for decades, with a recent resurgence of efforts investigating complex emergent phenomena near competing orders. Understanding the strong phonon anharmonicity in STO is of central importance to gain a deeper microscopic understanding of its unusual thermal transport properties, including hydrodynamic transport [1,2], effects of distortions [3], and the recently reported thermal Hall effect [4,5], as well as coupling of atomic dynamics to superconductivity [6–10], strain induced ferroelectricity [11], temperature-dependent electron-phonon coupling [12], and potential application in thermoelectrics [13,14]. Moreover, recent studies suggest an enhancement of superconductivity in FeSe films via the interaction with STO substrate phonons [15,16]. Of central importance, the strongly anharmonic lattice dynamics in STO reflect its incipient ferroelectric (FE) behavior, suppressed by quantum paraelectric fluctuations near a quantum critical point (QCP) [17–21]. Further complexity in dynamics arises from competition between FE and antiferrodistortive (AFD) orders [17,22–24].

Fundamentally, signatures of anharmonicity in solids are encoded and often analyzed through the frequency shifts and lifetime broadening (linewidths) of phonon modes in reciprocal space. Such shifts and linewidths are intrinsically temperature dependent as phonon occupations increase with T, and have triggered extensive research over the past decade to understand and control thermal transport properties of solids. While useful, phonon linewidths and shifts only inform us indirectly about real-space atomic motions. On the other hand, still in the phonon picture, the polarization eigenvectors provide an intuitive real-space understanding of collective ionic motions, which can be related to the electronic bonding to rationalize the sources of anharmonicity. Here, we show how phonon anharmonicity in STO is reflected in its T-dependent phonon eigenvectors, causing striking anomalies in $S(\mathbf{Q}, E)$ intensities measured with inelastic neutron scattering (INS), in particular the disappearance of transverse acoustic (TA) branches.

The ABO_3 perovskite structure exhibits inherent instabilities with respect to tilts and rotations of BO_6 octahedra and off-centering of ions. Intrinsically, these instabilities arise from anharmonic potential energy surfaces that induce soft-mode transitions. Perovskites exhibit a cubic structure at high temperature, and tend to distort to lower-symmetry phases on cooling [18,25], through BO_6 rotations and tilts, and off-centering of B cations inducing ferroelectric order [18,26]. Those transitions typically represent small distortions and involve soft phonon modes [25–28]. In $SrTiO_3$ the (incipient) FE instability originates from a doubly degenerate Γ point TO mode, moving cations and anions in opposite ways. The AFD instability involves oxygen octahedra rotations, in opposite directions in adjacent unit cells, corresponding to the lowest phonon branches at the R point of the Brillouin zone (BZ). The AFD phase transition occurs at ~105 K, lowering the symmetry from cubic to tetragonal on cooling, with R-point phonons

condensing [25]. In parallel, the zone-center transverse optic (TO) FE mode continually softens on cooling but never fully condenses, leaving the FE distortion incipient. While a Curie-Weiss fit predicts condensation at $T_C \sim 37$ K, the FE mode frequency plateaus at about ~2 meV below ~30 K [29,30], reflecting the nearby QCP [17–20].

Phonons in $SrTiO_3$ have previously been investigated with triple-axis INS at a limited number of $\mathbf{Q}$ vectors and with Raman spectroscopy at Γ [25,30–36]. Shirane and Yamada in particular reported a striking anomalous temperature dependence of the phonon intensity of a TA phonon at low T [30]. However, the anomaly was reported at a single $\mathbf{Q}$ point as a result of limitations of the triple-axis INS technique, and the observations could not be rationalized, remaining puzzling to this day.

Numerous experimental and theoretical studies have investigated the AFD-FE coupling [17,24], quantum fluctuation effects [22,23], electrical field and stress effects [37–39], anharmonic phonon renormalizations and linewidths [3,40,41], as well as thermal conductivity [3,12,42]. However, the T dependence of phonon eigenvectors has not been quantified nor analyzed in detail, which is crucial to understand the anomalous INS intensities in $SrTiO_3$. In this Letter, we explain the source of this striking behavior based on time-of-flight INS over extended $\mathbf{Q}$ volumes and first-principles simulations including anharmonic effects explicitly. The phonon softening and intensity anomalies in $S(\mathbf{Q}, E)$ are clearly resolved and mapped across $\mathbf{Q}$ space, and quantitatively reproduced and rationalized by simulations, solving a longstanding puzzle and providing new insights into the origins of anharmonicity in this important quantum paraelectric.

Single-crystal INS experiments were performed with the Hybrid Spectrometer (HYSPEC) [43] at the Spallation Neutron Source (SNS), and the HB-3 triple-axis spectrometer (TAS) at the High Flux Isotope Reactor (HFIR) at Oak Ridge National Laboratory. In HYSPEC experiments, a high-quality single crystal (mass = 15 g, mosaic < 0.25°) was aligned in the HHL scattering plane and measured with $E_i = 27$ and 15 meV at temperatures $2 < T < 300$ K. At each T, the four-dimensional $S(\mathbf{Q}, E)$ was mapped over multiple BZs by rotating the crystal over a wide angular range ($\mathbf{Q}$ space coverage illustrated in Supplemental Material [44] Fig. S4). Here, $\mathbf{Q}$ and $E = \hbar\omega$ denote the momentum and energy transfer from the neutrons to the sample, respectively. In TAS experiments, the same crystal was mounted on HHL plane and measured in constant-$E_f = 14.7$ meV mode. An additional 6.1 g crystal was aligned in the HK0 plane, and measured with $E_f = 30.5$ meV. TAS measurements used collimation settings of $48' \times 20' \times 20' \times 120'$.

First-principles phonon calculations were performed for both the cubic and tetragonal phases. We note that regular density-functional theory (DFT) phonon calculations based on the harmonic approximation yield unphysical results for

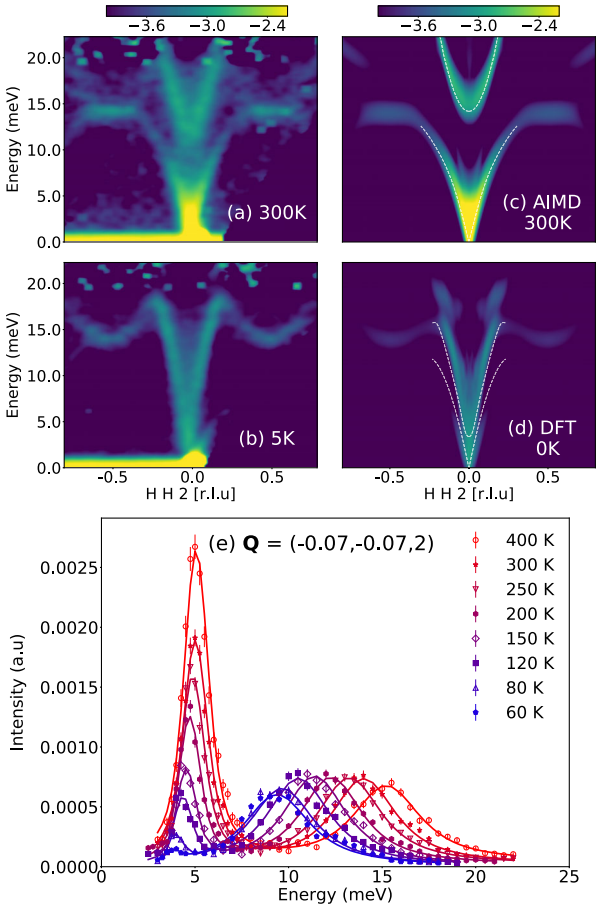

FIG. 1. Temperature dependence of $S(\boldsymbol{Q}, E)$ in $SrTiO_3$ showing disappearance of the TA branch at low T. (a) and (b) INS data from HYSPEC; (c) and (d) simulation results. Simulation for 300 K (c) is from the AIMD + TDEP method on the cubic phase, while the DFT result in (d) is from harmonic phonon calculation in tetragonal phase. In (a)–(d), $S(\boldsymbol{Q}, E)$ intensities from both INS and simulations are integrated over ±0.05 rlu along [0,0,1], and over ±0.1 rlu along [1,-1,0]. Intensity is plotted on a $\log_{10}$ scale. (e) HB-3 energy scans at $\boldsymbol{Q} = (-0.07, -0.07, 2)$ at different temperatures. The original data are markers, and solid lines are the fitted curves.

the cubic phase, which is dynamically unstable with instabilities at both Γ and R points (Supplemental Material [44] Fig. S1), in agreement with previous harmonic calculations [24,51–53]. However, both distortions are suppressed by anharmonic renormalization of these modes a high T [12,40–42,54,55]. In this study, we combine *ab initio* molecular dynamics (AIMD) with the temperature-dependent effective potential (TDEP) method to extract renormalized effective force constants at 120, 200, and 300 K for the cubic phase [54,55]. AIMD simulations were performed using VASP [56–58], within the generalized gradient approximation (GGA) in the Perdew-Burke-Ernzerhof (PBE) parametrization [59]. For the tetragonal phase, dynamically stable in the harmonic approximation, harmonic DFT calculations and the finite displacement

approach were used as implemented in Phonopy [60] (details in Supplemental Material [44], Secs. I and II).

Slices through $S(\mathbf{Q}, E)$ from HYSPEC are compared with simulations in Figs. 1(a)–1(d) and 2. Both INS data and simulations show the pronounced softening of the ferroelectric TO mode at Γ on cooling, congruent with incipient FE. Strikingly, as the FE mode softens, the intensity of $S(\mathbf{Q}, E)$ is dramatically suppressed over large portions of the TA branches around $\mathbf{Q} = (2, 2, 0)$ and (0,0,2), and nearly disappears at base temperature. Figure 1(e) shows the corresponding strongly anomalous behavior in 1D spectra at $\boldsymbol{Q} = (-0.07, -0.07, 2)$. Markers are the INS data while solid lines are fits convolved with the instrument resolution function [61]. It is obvious that the TA intensity is dramatically suppressed on cooling, while the TO peak shifts to lower frequency without much change in its intensity. A similar anomaly was reported by Yamada *et al.* at $\boldsymbol{Q} = (4, 0.1, 0)$, but has so far remained unexplained [30]. Additional HB-3 energy scans at different $\boldsymbol{Q}$ are shown in the Supplemental Material [44] Figs. S7(a)–S7(d). It is worthwhile to point out that, for INS on harmonic phonons, modes of lower energy should retain more intensity at low T than higher-energy ones, owing to Bose-Einstein statistics, and opposite to the present observation [62].

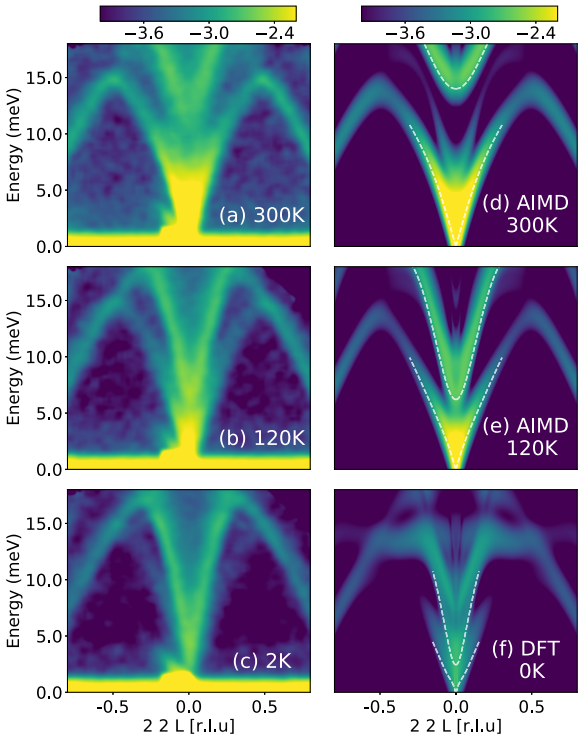

FIG. 2. $S(\boldsymbol{Q}, E)$ of $SrTiO_3$ along $\boldsymbol{Q} = [2\,2\,L]$ directions at different temperatures. Panels (a)–(c) show the INS data from HYSPEC at 300, 120, and 2 K. (d)–(f) Simulation results for the AIMD and TDEP method on the cubic phase at 300 (d) and 120 K (e), and DFT harmonic calculation on the tetragonal phase (f). $S(\boldsymbol{Q}, E)$ intensities from both INS and simulations are integrated over ±0.05 rlu along [1,1,0], and over ±0.1 rlu along $[1, -1, 0]$ and results are plotted in a $\log_{10}$ scale.

Our INS data also show a significant anomalous softening (energy decrease) of the TA branches on cooling, as seen in Fig. 1(e) and Supplemental Material [44] Figs. S7(c)–S7(e), which is captured by our renormalized phonon simulations, shown in Supplemental Material [44] Fig. S1. This anomalous softening of TA frequencies and group velocities (v_g) on cooling (counter to normal quasiharmonic trend) is also expected to directly impact the thermal conductivity, $\kappa \propto v_g^2$. Further, the renormalization of dispersions also impacts the phase space for anharmonic phonon-phonon scattering, as described in the Supplemental Material [44]. We note that anharmonic couplings between TA and TO modes were discussed in other ferroelectric incipient perovskites [63–66], although without clear effects on INS intensities in those cases.

For quasiharmonic phonons, the frequency ω depends only on volume, but not explicitly on temperature. Experimentally and theoretically, many studies have focused on investigating the T dependence of phonon frequencies, $\omega(T)$, and the phonon linewidths [$2\Gamma(T) \propto \tau^{-1}(T)$] to probe phonon anharmonicity beyond the quasiharmonic effects associated with volume change. Importantly, the coherent phonon scattering cross section measured with INS is directly proportional to the dynamical structure factor $S(\boldsymbol{Q}, E)$ [62]:

$$S(\boldsymbol{Q}, E) \propto |F(\boldsymbol{Q})|^2 \frac{(n+1)}{\omega},$$
$$F(\boldsymbol{Q}) = \sum_j (\boldsymbol{Q} \cdot e_j) \frac{b_j}{\sqrt{M_j}} e^{i\boldsymbol{Q}\cdot\boldsymbol{R}_j} e^{-W_j}, \qquad (1)$$

in which j refers the jth atom in the unit cell, e_j is its eigenvector component, b_j the neutron scattering length, M_j the atomic mass, R_j is the atomic position, and W_j the Debye-Waller factor. Most investigations of phonon anharmonicity in materials have focused on temperature shifts of frequencies $\omega(T)$, which lead to T changes in INS measurements via $(n+1)/\omega(T)$. However, and crucial here, thermal renormalization also affects the phonon eigenvectors, which become T dependent [$e_j(T)$] and thus modulate $F(\boldsymbol{Q}, T)$, providing another window into anharmonic effects on atomic vibrations. We proceed to show how anharmonic effects on $e_j(T)$ lead to the spectacular thermal changes of INS intensities seen in Figs. 1 and 2.

In order to gain a more quantitative understanding, we examine 1D spectra from which we extract the T-dependent intensities of specific modes (see methods in Supplemental Material [44]). In Fig. 3(a), the measured T-dependent intensity of the TA phonon at $\boldsymbol{Q} = (-0.07, -0.07, 2)$ is compared with $(n+1)/\omega(T)$, after scaling to coincide at 300 K (results for additional TA and TO phonons are shown in Supplemental Material [44] Figs. S8 and S9). From these

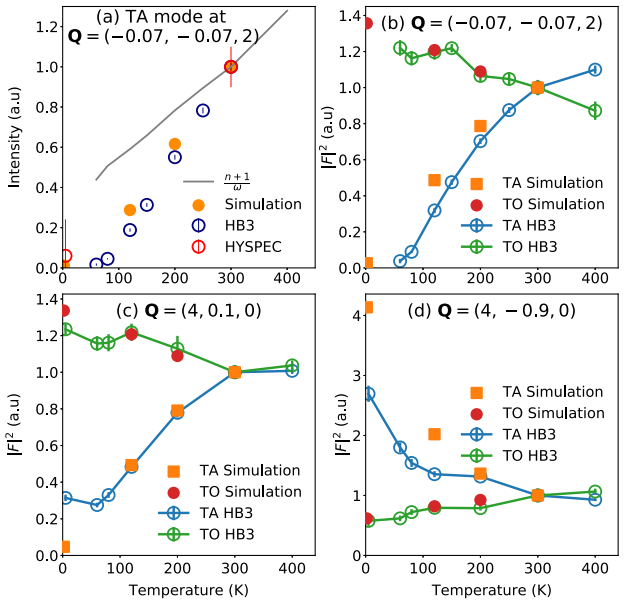

FIG. 3. (a) Intensity of TA phonons with temperature. On cooling, the TA intensity falls below $(n+1)/\omega$, indicating that $|F|^2$ decreases at low T. (b)–(d) $|F|^2$ of TA and TO modes of $SrTiO_3$ at different temperature at different Q points. At $\boldsymbol{Q} = (2, 2, 0.1), (-0.07, -0.07, 2)$, and (4,0.1,0), $|F|^2$ of TA decreases on cooling and that of TO increases. At $\boldsymbol{Q} = (4, -0.9, 0)$, $|F|^2$ of TA increases on cooling while that of TO decreases due to the change in eigenvector phase. An arbitrary scaling was chosen to bring data to coincide at 300 K. Small error bars are inside markers.

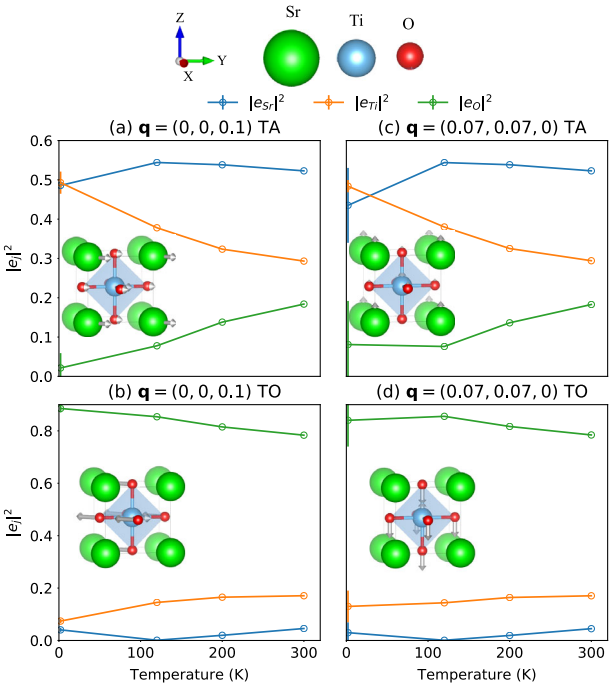

FIG. 4. The TA and TO eigenvector modules of different atoms vs temperature. The 300, 200, and 120 K data are from the AIMD and TDEP method on the cubic phase, and the 0 K data are from harmonic phonon calculation on the tetragonal phase. For both reduced wave vector $\boldsymbol{q}$, $|e_{Ti}|$ of TA increases and $|e_O|$ of TA decreases as cooling. $|e_{Ti}|$ of TO decreases and $|e_O|$ of TA increases as cooling. For 0 K simulation, the tetragonal phase has anisotropy, and the differences between orientations are shown as error bars.

figures, it is obvious that intensities of TA and TO modes exhibit clear discrepancies with Eq. (1) for quasiharmonic phonons. This implies that the structure factors of TA and TO modes exhibit an intrinsic temperature dependence. On the other hand, the simulation results in Fig. 3(a), corresponding to the product of the simulated T-dependent $|F|^2(T)$ and the experimental $(n+1)/\omega(T)$, captures the trends very well. To further analyze anharmonic effects, $|F(\boldsymbol{Q}, T)|$ for the TA and TO modes are plotted in Figs. 3(b)–3(d) (scaled to coincide at 300 K). In Figs. 3(b) and 3(c), the $|F|$ of TA strongly decreases on cooling and $|F|$ of TO increases on cooling, while in Fig. 3(d), $|F|$ follows the opposite trend, which we now rationalize.

The evolution of $|F(\boldsymbol{Q})|$ with T reflects changes in the respective phonon eigenvectors. Since $\sum_j |e_j|^2 = 1$, it is apparent that the relative magnitudes of components of e_j for Sr, Ti, and O atoms determine $|F(\boldsymbol{Q}, T)|^2$. The eigenvector components obtained from our simulations are plotted in Fig. 4. It is obvious that for the TA mode, $|e_{Ti}|$ increases on cooling, while $|e_O|$ decreases. The TO eigenvector components follow an opposite trend. Considering that Ti has a negative neutron scattering length, $b_{\text{coh}} = -3.438$ fm (femtometers), while Sr and O have positive scattering lengths ($b_{\text{coh}} = 7.02$ and 5.803 fm, respectively, see Supplemental Material [44]), we can understand that when $|e_{Ti}|$ increases, the total $|F(\boldsymbol{Q})|$ decreases. Thus, dramatic TA and TO intensity change are observed at $\mathbf{Q} = (2, 2, 0.1), (4, 0.1, 0)$, and $(-0.07, -0.07, 2)$. The agreement between our modeling and measurements was further tested by checking the effect of the change in spatial phase across a BZ. We can compare $\mathbf{Q} = (4, -0.9, 0)$ and (4,0.1,0), which are symmetry equivalent and thus have the same phonon eigenvector magnitudes but opposite phases for the Ti atom and two O atoms motions. As can be seen in Fig. 3(d), the measured $|F(\boldsymbol{Q})|$ of the TA mode at $(4, -0.9, 0)$ actually increases on cooling, opposite to the behavior at (4,0.1,0), and this is also well captured in our simulations. We thus stress that the different experimental trends at many $\mathbf{Q}$ vectors spanning multiple BZs are all accounted for with our simulations.

It is worth noting that the transverse modes exhibiting anomalous phonon intensities along $\Gamma - X$ or $\Gamma - M$ are all polarized in x or symmetrically equivalent directions in real space. On the other hand, the transverse modes along $\Gamma - R$ (Supplemental Material [44], Fig. S5) or $(2 - H, 2 + H, 0)$ [30] behave normally. To clarify the origin of this anisotropy, we inspected the dynamical matrix (Supplemental Material [44], Sec. IX). For a simple cubic system with 5 atoms in the unit cell, the dynamical

matrix is a 15×15 Hermitian matrix. Along high symmetry directions, it can be block diagonalized [34,63]. It is found that the transverse modes polarized along x (or y, z) are determined by a block 5×5 matrix (A_2), which is derived solely from diagonal components of force constants and influenced mostly by the Ti-O interaction along [100].

We note that our model is based on a renormalized phonon description, with the T dependence arising from the anharmonicity of the crystal potential energy surface. Thus sampling of larger atomic displacements results in stronger renormalization (e.g., stiffening of the zone-center FE TO mode). Interestingly, simulations within the quasiharmonic approximation (QHA) in the cubic phase exhibit a related, yet unphysical trend in INS intensities. Upon increasing the lattice constant, the TO phonon softens and TA intensities are suppressed (Supplemental Material [44], Fig. S11). However, since the lattice actually contracts on cooling, the QHA prediction is the opposite of experimental observations. This highlights the importance of including intrinsic anharmonic effects in perovskites. In agreement with reported experiments [38,39] and simulations [24,67], pressure (compression) stiffens the anharmonic potential well and thus suppresses the FE instability. At the same time, the change in phonon eigenvectors leads to intensity modulation. As is well known, the FE instability in perovskites is strongly sensitive to the hybridization of Ti and O orbitals [68,69]. Temperature and pressure both modulate the overlap of Ti and O electronic orbitals and thus interatomic force constants. As the system approaches the FE transition, either upon cooling or volume expansion (in QHA), the longitudinal Ti-O interatomic force constants (FC) weaken, which results in the FE mode softening and eigenvector renomalization. When the compensating force constants no longer can prevent the instability, the phase transition occurs [28,70]. By adjusting the FC of the shortest Ti-O bonds, keeping other the FC unchanged, the phonon softening and intensity anomaly is also reproduced (see Supplemental Material [44], Sec. XII), confirming the critical role of this T-dependent FC. This also explains why anomalous phonon intensities are more pronounced for modes polarized along x, since these directly involve atomic motions along the Ti-O bond.

In conclusion, a strongly anomalous T dependence of phonon intensities and phonon energies was observed in $SrTiO_3$ across multiple directions in large $S(\mathbf{Q}, E)$ volumes mapped with state-of-the-art INS experiments. This was rationalized based on first-principles simulations accounting for anharmonic renormalization of phonon frequencies and eigenvectors, which capture the experimental trend quantitatively. By analyzing the T dependence of the force constants and the dynamical structure factor, we identified how the anharmonic renormalization of eigenvectors, particularly Ti and O motions, is responsible for this striking effect. Moreover, we show that the strongly anharmonic modes are primarily determined by the diagonal force constants in the Ti-O interaction. These results establish how a striking T dependence of phonon intensities beyond the harmonic picture can be quantitatively measured with INS mapping of $S(\mathbf{Q}, E)$ volumes, providing direct insights into the anharmonic behavior of phonon eigenvectors, and also show how first-principles simulations including anharmonic effects can reproduce and rationalize such effects. The identified T dependence of force constants and dispersions will also be important to quantitatively rationalize unusual thermal transport in $SrTiO_3$. Our methods directly carry over to the study of numerous other anharmonic materials.

We thank Olle Hellman for providing the TDEP software. We thank Andrei Savici and Melissa Graves-Brook for support and Jiawang Hong and Huibo Cao for helpful discussions. Neutron scattering measurements were supported by the U.S. Department of Energy, Office of Science, Basic Energy Sciences, Materials Sciences and Engineering Division, under the Early Career Award No. DE-SC0016166. Data analysis and first-principles modeling were supported by the U.S. Department of Energy, Office of Science, Basic Energy Sciences, Materials Sciences and Engineering Division, under Award No. DE-SC0019978. The research at Oak Ridge National Laboratory's Spallation Neutron Source and High Flux Isotope Reactor was sponsored by the Scientific User Facilities Division, Office of Basic Energy Sciences, US DOE. Theoretical calculations were performed using resources of the National Energy Research Scientific Computing Center, A U.S. DOE Office of Science User Facility supported by the Office of Science of the U.S. Department of Energy under Contract No. DE-AC02-05CH11231.

*olivier.delaire@duke.edu

[1] V. Martelli, J. L. Jiménez, M. Continentino, E. Baggio-Saitovitch, and K. Behnia, Phys. Rev. Lett. **120**, 125901 (2018).
[2] P. Torres, J. A. Seijas-Bellido, C. Escorihuela-Sayalero, J. Íñiguez, and R. Rurali, Phys. Rev. Mater. **3**, 044404 (2019).
[3] A. O. Fumega, Y. Fu, V. Pardo, and D. Singh, arXiv:1909.12193.
[4] X. Li, B. Fauqué, Z. Zhu, and K. Behnia, Phys. Rev. Lett. **124**, 105901 (2020).
[5] J. Chen, S. Kivelson, and X. Sun, arXiv:1910.00018.
[6] B. S. De Lima, M. S. Da Luz, F. S. Oliveira, L. M. S. Alves, C. A. M. Dos Santos, F. Jomard, Y. Sidis, P. Bourges, S. Harms, C. P. Grams *et al.*, Phys. Rev. B **91**, 045108 (2015).
[7] J. R. Arce-Gamboa and G. G. Guzmán-Verri, Phys. Rev. Mater. **2**, 104804 (2018).
[8] D. van der Marel, F. Barantani, and C. W. Rischau, Phys. Rev. Research **1**, 013003 (2019).
[9] K. Ahadi, L. Galletti, Y. Li, S. Salmani-Rezaie, W. Wu, and S. Stemmer, Sci. Adv. **5**, eaaw0120 (2019).

[10] Y. Tomioka, N. Shirakawa, K. Shibuya, and I. H. Inoue, Nat. Commun. **10**, 738 (2019).
[11] D. Lee, H. Lu, Y. Gu, S. Y. Choi, S. D. Li, S. Ryu, T. R. Paudel, K. Song, E. Mikheev, S. Lee *et al.*, Science **349**, 1314 (2015).
[12] J. J. Zhou, O. Hellman, and M. Bernardi, Phys. Rev. Lett. **121**, 226603 (2018).
[13] S. R. Popuri, A. J. M. Scott, R. A. Downie, M. A. Hall, E. Suard, R. Decourt, M. Pollet, and J. W. G. Bos, RSC Adv. **4**, 33720 (2014).
[14] Z. Lu, H. Zhang, W. Lei, D. C. Sinclair, and I. M. Reaney, Chem. Mater. **28**, 925 (2016).
[15] J. J. Lee, F. T. Schmitt, R. G. Moore, S. Johnston, Y. T. Cui, W. Li, M. Yi, Z. K. Liu, M. Hashimoto, Y. Zhang *et al.*, Nature (London) **515**, 245 (2014).
[16] S. Gerber, S. L. Yang, D. Zhu, H. Soifer, J. A. Sobota, S. Rebec, J. J. Lee, T. Jia, B. Moritz, C. Jia *et al.*, Science **357**, 71 (2017).
[17] S. Field, N. Venturi, and F. Nori, Phys. Rev. Lett. **74**, 2587 (1995).
[18] W. Zhong and D. Vanderbilt, Phys. Rev. B **53**, 5047 (1996).
[19] H. Taniguchi, M. Itoh, and T. Yagi, Phys. Rev. Lett. **99**, 017602 (2007).
[20] S. E. Rowley, L. J. Spalek, R. P. Smith, M. P. M. Dean, M. Itoh, J. F. Scott, G. G. Lonzarich, and S. S. Saxena, Nat. Phys. **10**, 367 (2014).
[21] D. E. Grupp and A. M. Goldman, Phys. Rev. Lett. **78**, 3511 (1997).
[22] D. Vanderbilt and W. Zhong, Ferroelectrics **206**, 181 (1998).
[23] N. Sai and D. Vanderbilt, Phys. Rev. B **62**, 13942 (2000).
[24] U. Aschauer and N. A. Spaldin, J. Phys. Condens. Matter **26**, 122203 (2014).
[25] G. Shirane and Y. Yamada, Phys. Rev. **177**, 858 (1969).
[26] G. Shirane, J. Axe, J. Harada, and J. Remeika, Phys. Rev. B **2**, 155 (1970).
[27] E. Farhi, A. K. Tagantsev, R. Currat, B. Hehlen, E. Courtens, and L. Boatner, Eur. Phys. J. B **15**, 615 (2000).
[28] P. Ghosez, E. Cockayne, U. V. Waghmare, and K. M. Rabe, Phys. Rev. B **60**, 836 (1999).
[29] K. A. Müller, W. Berlinger, and E. Tosatti, Z. Phys. B **84**, 277 (1991).
[30] Y. Yamada and G. Shirane, J. Phys. Soc. Jpn. **26**, 396 (1969).
[31] R. A. Cowley, W. J. L. Buyers, and G. Dolling, Solid State Commun. **7**, 181 (1969).
[32] T. Riste, E. J. Samuelsen, K. Otnes, and J. Feder, Solid State Commun. **9**, 1455 (1971).
[33] J. Harada, J. D. Axe, and G. Shirane, Acta Crystallogr. Sect. A **26**, 608 (1970).
[34] R. A. Cowley, Phys. Rev. **134**, A981 (1964).
[35] J. F. Scott and H. Ledbetter, Z. Phys. B **104**, 635 (1997).
[36] K. Inoue and N. Asai, J. Phys. (Paris), Colloq. **42**, C6-430 (1981).
[37] P. A. Fleury and J. M. Worlock, Phys. Rev. **174**, 613 (1968).
[38] H. Uwe and T. Sakudo, Phys. Rev. B **13**, 271 (1976).
[39] M. Guennou, P. Bouvier, J. Kreisel, and D. Machon, Phys. Rev. B **81**, 054115 (2010).
[40] T. Tadano and S. Tsuneyuki, Phys. Rev. B **92**, 054301 (2015).
[41] T. Tadano and S. Tsuneyuki, J. Phys. Soc. Jpn. **87**, 041015 (2018).
[42] L. Feng, T. Shiga, and J. Shiomi, Appl. Phys. Express **8**, 071501 (2015).
[43] B. Winn, U. Filges, V. O. Garlea, M. Graves-Brook, M. Hagen, C. Jiang, M. Kenzelmann, L. Passell, S. M. Shapiro, X. Tong *et al.*, EPJ Web Conf. **83**, 03017 (2015).
[44] See Supplemental Material at http://link.aps.org/supplemental/10.1103/PhysRevLett.124.145901 for details which includes Refs. [45–50].
[45] H. Fujishita, Y. Shiozaki, and E. Sawaguchi, J. Phys. Soc. Jpn. **46**, 581 (1979).
[46] J. Feder and E. Pytte, Phys. Rev. B **1**, 4803 (1970).
[47] W. Li, J. Carrete, N. A. Katcho, and N. Mingo, Comput. Phys. Commun. **185**, 1747 (2014).
[48] E. F. Steigmeier, Phys. Rev. **168**, 523 (1968).
[49] E. Fischer and E. Hegenbarth, Ferroelectr. Lett. Sect. **5**, 21 (1985).
[50] A. Togo, L. Chaput, and I. Tanaka, Phys. Rev. B **91**, 094306 (2015).
[51] A. I. Lebedev, Phys. Solid State **51**, 362 (2009).
[52] R. A. Evarestov, E. Blokhin, D. Gryaznov, E. A. Kotomin, and J. Maier, Phys. Rev. B **83**, 134108 (2011).
[53] R. Wahl, D. Vogtenhuber, and G. Kresse, Phys. Rev. B **78**, 104116 (2008).
[54] O. Hellman, I. A. Abrikosov, and S. I. Simak, Phys. Rev. B **84**, 180301(R) (2011).
[55] O. Hellman, P. Steneteg, I. A. Abrikosov, and S. I. Simak, Phys. Rev. B **87**, 104111 (2013).
[56] G. Kresse and J. Hafner, Phys. Rev. B **47**, 558 (1993).
[57] G. Kresse and J. Furthmüller, Phys. Rev. B **54**, 11169 (1996).
[58] G. Kresse and J. Furthmüller, Comput. Mater. Sci. **6**, 15 (1996).
[59] J. P. Perdew, K. Burke, and M. Ernzerhof, Phys. Rev. Lett. **77**, 3865 (1996).
[60] A. Togo and I. Tanaka, Scr. Mater. **108**, 1 (2015).
[61] A. Zheludev, Reslib 3.4 manual https://neutron.ethz.ch/research/resources/reslib.html (2007).
[62] G. L. Squires, *Introduction to the Theory of Thermal Neutron Scattering* (Cambridge University Press, Cambridge, England, 2012).
[63] J. D. Axe, J. Harada, and G. Shirane, Phys. Rev. B **1**, 1227 (1970).
[64] M. D. Fontana, G. E. Kugel, L. Foussadier, W. Kress, and D. Rytz, Europhys. Lett. **23**, 427 (1993).
[65] L. Foussadier, M. D. Fontana, and W. Kress, J. Phys. Condens. Matter **8**, 1135 (1996).
[66] A. Bussmann-Holder, J. Phys. Condens. Matter **24**, 273202 (2012).
[67] I. A. Kornev, L. Bellaiche, P. Bouvier, P.-E. Janolin, B. Dkhil, and J. Kreisel, Phys. Rev. Lett. **95**, 196804 (2005).
[68] R. E. Cohen, Nature (London) **358**, 136 (1992).
[69] Y. A. Abramov, V. G. Tsirelson, V. E. Zavodnik, S. A. Ivanov, and I. D. Brown, Acta Crystallogr. Sect. B **51**, 942 (1995).
[70] Y. Xie, H. Yu, G. Zhang, and H. Fu, J. Phys. Condens. Matter **20**, 215215 (2008).